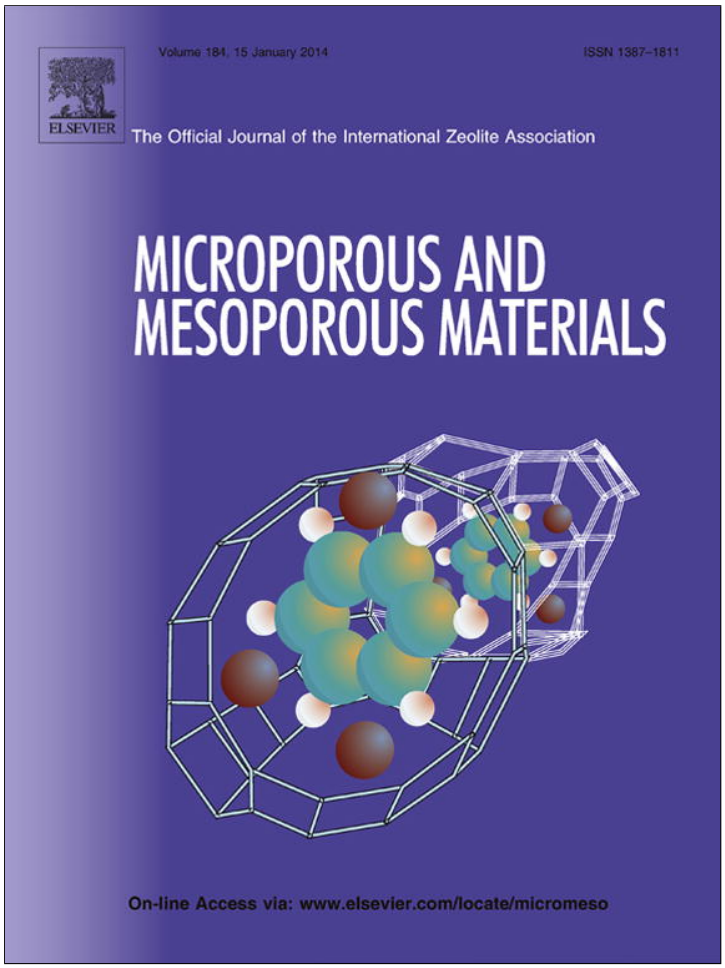

Microporous and Mesoporous Materials 184 (2014) 15–20

Contents lists available at ScienceDirect

Microporous and Mesoporous Materials

journal homepage: www.elsevier.com/locate/micromeso

Syntheses, structures, thermal stabilities and gas sorption properties of two rod-based microporous lead(II) polycarboxylate coordination frameworks

Ying Zhang [a], Jue Wang [a], Xiufen Yan [a], Xiaoqing Liu [a], Hu Zhou [b,c], Aihua Yuan [a,*]

[a] School of Biology and Chemical Engineering, Jiangsu University of Science and Technology, Zhenjiang 212003, PR China
[b] School of Material Science and Engineering, Jiangsu University of Science and Technology, Zhenjiang 212003, PR China
[c] SiYang Diesel Engine Manufacturing Co., Ltd, Zhenjiang 212003, PR China

ARTICLE INFO

Article history:
Received 8 May 2013
Received in revised form 21 September 2013
Accepted 29 September 2013
Available online 7 October 2013

Keywords:
Metal–organic framework
Lead
Polycarboxylates
Gas sorption

ABSTRACT

Two new lead(II)–organic frameworks $Pb_2(\mu_4\text{-}O)(bdc)\cdot DMF$ (**1**) and Pb(ndc)(DMF) (**2**) (H_2bdc = 1,4-benzenedicarboxylate, H_2ndc = 2,6-naphthalenedicarboxylate, DMF = *N*,*N*′-dimethylformamide) were prepared through solvothermal methods. Single-crystal X-ray diffraction analysis indicated that compounds **1** and **2** exhibit rod-based three-dimensional (3D) porous frameworks with 1D channels. The carboxylate groups in both compounds adopt different types of coordination modes, and the coordination geometries of lead(II) centers in compound **1** and **2** are hemidirected and holodirected, respectively. Gas sorption results showed that compound **1** has moderate uptakes for nitrogen and hydrogen gases, owing to the existence of micropores in structures.

1. Introduction

In recent years, metal-organic frameworks (MOFs) with high specific surface areas and permanent porosities have attracted extensive attention because of their potential applications in gas storage [1], separation [2], drug delivery [3], catalysis [4], and so on. The three-dimensional (3D) porous MOFs with intriguing structural topology have become excellent candidates for gas storage materials depending on the high specific surface areas, valid holes and firm bodies. Up to now, a large number of such MOFs were investigated for gas sorption properties with the center metal ions M^{2+} (M = Ni, Co, Mg, Mn, Zn, etc), while lead(II)-organic frameworks have rarely been studied on porosities and gas sorption properties.

Lead(II), the heavy toxic metal, is easy to extract, dense, highly malleable and stable to corrosion. The widespread use in industrial application mainly for battery making and recycling, oil refining, paint manufacturing has caused environmental contamination. To better know, the toxic mechanism, it is vital to understand its coordination properties: the lone pair of electrons, coordination number and coordination geometry. Different from transition metals, the main group metal lead(II) with large ionic radius and the stereochemically effective lone pair electrons offers variable possibilities of coordination numbers, and has been employed to build versatile geometries of holo- or hemi-directed, and therefore highly-linked lead(II)-organic frameworks [5]. It is interesting to investigate the perplexing architectures of 3D highly-linked lead(II) MOFs and especially of much significance to explore the gas storage of them. Unfortunately, to our knowledge, gas sorption properties of only three Pb-organic frameworks were investigated to date, [Pb(SDBA)] (H_2SDBA = 4,4′-sulfonyldibenzoic acid) [6], $[PbL_2]\cdot 2DMF\cdot 6H_2O$ and $[PbL_2]\cdot DMF\cdot 2H_2O$ (HL_2 = *N*-(4-carboxyphenyl)isonicotinamide 1-oxide) [7]. Among them, the methane sorption of [Pb(SDBA)] accumulates to 2 wt% at 183 K, 2.2 atm but no uptake of nitrogen at low pressure (1 atm). In addition, the H_2O vapor adsorption isotherms of desolvated $[PbL_2]\cdot 2DMF\cdot 6H_2O$ and $[PbL_2]\cdot DMF\cdot 2H_2O$ display preferential behaviors over CO_2 due to the hydrophilic nature of the channel.

The successful syntheses of these porous materials are mainly based on the concept of network design [8], in which the structures of organic ligands have played a key role [9]. Among them, mixed organic ligands composing of polycarboxylic acids (O-donor) and N-donor ligands have been used recently to construct porous MOFs [10–12], owing to their rich coordination modes with metal centers. Recently, both the O-donor carboxylate acids (1,4-benzenedicarboxylate (H_2bdc) or 2,6-naphthalenedicarboxylate (H_2ndc)) and the N-donor ligands (pyrazine, 4,4′-azopyridine (azpy)) were employed as mixing ligands by our group to react with lead(II) ions in *N*,*N*′-dimethylformamide (DMF) through the solvothermal

* Corresponding author. Tel.: +86 511 85638920; fax: +86 511 85635850.
E-mail address: aihuayuan@163.com (A. Yuan).

1387-1811/$ - see front matter © 2013 Elsevier Inc. All rights reserved.
http://dx.doi.org/10.1016/j.micromeso.2013.09.035

method, in order to construct 3D porous lead(II) MOFs with intriguing topologies and permanent porosities. Unexpectedly, the N-donor ligands pyrazine and azpy did not coordinate with lead(II) centers, and then two new porous MOFs $Pb_2(\mu_4\text{-}O)(bdc)\cdot DMF$ (**1**) and Pb(ndc)(DMF) (**2**) were isolated instead. In this contribution, we reported the syntheses, crystal structures and thermal stabilities of both materials, together with gas sorption properties of compound **1**. To our knowledge, nitrogen and hydrogen gas sorption behaviors of lead(II)-polycarboxylate frameworks have not been documented previously.

2. Experimental

2.1. Materials and physical measurements

1,4-Benzenedicarboxylate (H_2bdc) and 2,6-naphthalenedicarboxylate (H_2ndc), pyrazine, 4,4′-azopyridine (azpy), *N*,*N*′-dimethylamide (DMA), *N*,*N*′-dimethylformamide (DMF) and $Pb(NO_3)_2$ were purchased from J&K CHEMICA in a reagent grade and used without any purification. Infrared spectra as KBr pellets were recorded using Avatar Nicolet FT-1703x FT-IR spectrophotometer from 4000 to 400 cm^{-1}. Thermalgravimetric (TG) analyses were taken on a Pyris Diamond TGA analyzer at a heating rate of 10 °C min^{-1}. Powder X-ray diffraction (XRD) measurements were performed on a Shimadzu XRD-6000 diffractometer with CuK_α radiation. The nitrogen and hydrogen gas sorption isotherms were measured using an automatic volumetric adsorption equipment (ASAP 2020, Mircomeritics). Proceeding to gas sorption experiments, powder samples of compound **1** were activation at 180 °C under vacuum over 24 h. The adsorption and desorption isotherms of N_2 and H_2 were measured at 77 K.

2.2. Syntheses

2.2.1. Preparation of $Pb_2(\mu_4\text{-}O)(bdc)\cdot DMF$ (*1*)

A mixture of $Pb(NO_3)_2$ (0.1 mmol), H_2bdc (0.05 mmol), pyrazine (0.1 mmol) combined with 5 mL DMA and 5 mL DMF was stirred for 20 min at room temperature. Then the solution was heated to 140 °C at the rate of 1 °C min^{-1} in a 30 mL Teflon-lined stainless-steel vessel. After maintaining in 140 °C for 3 days, the solution was cooled to room temperature at the rate of 3 °C h^{-1}. The colorless block-shaped crystals was collected by filtration, washed with DMF, and then air-dried to give compound **1**. Yield: 45% (based on Pb salt). In fact, the absence of pyrazine has not resulted in the isolation of any crystals. The brands at 1544 and 1375 cm^{-1} in IR spectra are assigned to the asymmetric and symmetric stretching vibrations of aromatic ν(C–O). The brands at 824, 748 cm^{-1} are specified to the bending vibrations of aromatic ν(C–H).

2.2.2. Preparation of Pb(ndc)(DMF) (*2*)

A mixture of $Pb(NO_3)_2$ (0.1 mmol), H_2ndc (0.1 mmol), and azpy (0.1 mmol) in 10 mL DMF was stirred for 20 min at room temperature. Then the solution was heated at the rate of 1 °C min^{-1} in a 30 mL Teflon-lined stainless-steel vessel to 160 °C. After that it was heated for 3 days under autogenous pressure. Slow cooling of the resulting solution to room temperature at the rate of 3 °C h^{-1} afforded yellow block-shaped crystals. The crystalline product was collected by filtration, washed with DMF, and then air-dried to give compound **2**. Yield: 52% (based on Pb salt). Similar to compound **1**, no products were isolated in the absence of azpy for compound **2**. The brands at 1636, 1542 and 1387 cm^{-1} in spectra are assigned to the asymmetric and symmetric stretching vibrations of aromatic ν(C–O). The brands at 792 cm^{-1} are specified to the bending vibrations of aromatic ν(C–H).

Table 1
Crystallographic data and refinement details for compounds **1** and **2**.

Compounds	**1**	**2**
Chemical formula	$C_{11}H_{11}NO_6Pb_2$	$C_{15}H_{13}NO_5Pb$
Formula weight	667.59	494.45
Crystal system	Orthorhombic	Orthorhombic
Space group	$P2_12_12_1$	Pnma
a/Å	10.7932(12)	7.5502(16)
b/Å	12.1372(11)	20.1464(17)
c/Å	22.132(2)	10.3753(15)
α/°	90.00	90.00
β/°	90.00	90.00
γ/°	90.00	90.00
V/Å^3	2899.3 (5)	1578.18(4)
Z	8	4
Calculated density/g cm^3	3.059	2.081
μ/mm^{-1}	23.219	10.712
F(000)	2368	928
S	1.120	1.024
R_1, ωR_2 [$I > 2\sigma(I)$]	0.0387, 0.0878	0.0353, 0.0863
R_1, ωR_2 (all data)	0.0421, 0.0890	0.0502, 0.0924

Table 2
Selected bond lengths (Å) and angles (°) for compound **1**.

Compound **1**			
Pb1–O1	2.466(10)	Pb3–O2^{v}	2.411(9)
Pb1–O3^{vi}	2.626(10)	Pb3–O5	2.656(10)
Pb1–O9	2.310(10)	Pb3–O9	2.275(10)
Pb1–O10^{iii}	2.260(10)	Pb3–O10	2.259(10)
Pb2–O5	2.757(11)	Pb4–O4^{vi}	2.684(10)
Pb2–O7	2.388(10)	Pb4–O8	2.525(10)
Pb2–O9	2.297(10)	Pb4–O9	2.306(10)
Pb2–O10	2.358(11)	Pb4–O10^{iii}	2.324(10)
O10^{iii}–Pb1–O9	75.0(4)	O10–Pb3–O9	76.4(4)
O10^{iii}–Pb1–O1	91.5(4)	O10–Pb3–O2^{v}	91.5(4)
O9–Pb1–O1	85.1(4)	O9–Pb3–O2^{v}	80.4(3)
O10^{iii}–Pb1–O3^{vi}	96.7(4)	O10–Pb3–O5	81.2(4)
O9–Pb1–O3^{vi}	74.0(3)	O9–Pb3–O5	66.7(3)
O1–Pb1–O3^{vi}	154.6(4)	O2^{v}–Pb3–O5	147.1(3)
O9–Pb2–O10	74.1(4)	O9–Pb4–O10^{iii}	73.9(4)
O9–Pb2–O7	88.9(4)	O9–Pb4–O8	85.3(3)
O10–Pb2–O7	79.1(3)	O10^{iii}–Pb4–O8	81.4(3)
O9–Pb2–O5	64.6(3)	O9–Pb4–O4^{vi}	96.5(4)
O10–Pb2–O5	77.4(3)	O10^{iii}–Pb4–O4^{vi}	73.3(3)
O7–Pb2–O5	148.5(3)	O8–Pb4–O4^{vi}	152.9(3)

Symmetry code: (iii) $x + 1/2$, $-y + 3/2$, $-z + 2$; (v) x $-1/2$, $-y + 3/2$, $-z + 2$; (vi) $-x + 1/2$, $-y + 2$, $z + 1/2$.

Table 3
Selected bond lengths (Å) and angles (°) for compound **2**.

Compound **2**			
Pb1–O1	2.727(5)	Pb1–O2^{iv}	2.593(5)
Pb1–O1^{ii}	2.727(5)	Pb1–O2^{v}	2.593(5)
Pb1–O1^{iv}	2.507(5)	Pb1–O3	2.692(6)
Pb1–O1^{v}	2.507(5)	O1^{iv}–Pb1–O1	98.75(17)
O1^{iv}–Pb1–O1^{v}	79.8(2)	O1^{v}–Pb1–O1	155.23(5)
O1^{iv}–Pb1–O2^{iv}	50.77(13)	O2^{iv}–Pb1–O1	92.24(16)
O1^{v}–Pb1–O2^{iv}	105.14(16)	O2^{v}–Pb1–O1	149.39(13)
O1^{iv}–Pb1–O2^{v}	105.14(16)	O3–Pb1–O1	84.31(14)
O1^{v}–Pb1–O2^{v}	50.77(13)	O1^{iv}–Pb1–O1^{ii}	155.23(5)
O2^{iv}–Pb1–O2^{v}	88.4(2)	O1^{v}–Pb1–O1^{ii}	98.75(17)
O1^{iv}–Pb1–O3	71.68(14)	O2^{iv}–Pb1–O1^{ii}	149.39(13)
O1^{v}–Pb1–O3	71.68(14)	O2^{v}–Pb1–O1^{ii}	92.24(16)
O2^{iv}–Pb1–O3	121.12(12)	O3–Pb1–O1^{ii}	84.31(14)
O2^{v}–Pb1–O3	121.12(12)	O1–Pb1–O1^{ii}	72.2(2)

Symmetry codes: (ii) x, $-y + 1/2$, z; (iv) $x + 1/2$, y, $-z + 1/2$; (v) $x + 1/2$, $-y + 1/2$, $-z + 1/2$.

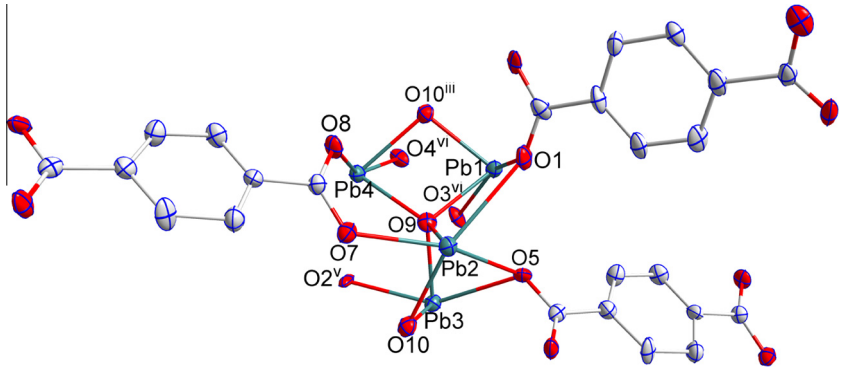

Fig. 1. ORTEP diagram of compound **1** with displacement ellipsoids drawn at 30% probability level. All hydrogen atoms and uncoordinated DMF molecules have been omitted for clarity. Symmetry code: (iii) $x + 1/2, -y + 3/2, -z + 2$; (v) $x-1/2, -y + 3/2, -z + 2$; (vi) $-x + 1/2, -y + 2, z + 1/2$.

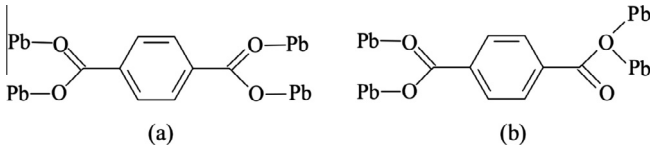

Scheme 1. The two coordination modes of bdc ligand in the structure of compound **1**.

2.3. Crystallographic data collection and structure determination

Diffraction data for compounds **1** and **2** were collected at 291(2) K on a Bruker Smart APEX II diffractometer equipped with Mo-K_α (λ = 0.71073 Å) radiation. Diffraction data analysis and reduction were performed within *SMART*, *SAINT* and *XPREP* [13] Correction for Lorentz, polarization and absorption effects were performed within *SADABS* [14]. Structures were solved using Patterson method within *SHELXS-97* and refined using *SHELXL-97* [15,16]. All non-hydrogen atoms were refined anisotropically. All hydrogen atoms were calculated at idealized positions and refined in a riding mode. The coordinated DMF molecule in compound **2** was disordered into two sites. The crystallographic data and refinement details of compounds **1** and **2** are given in Table 1. Selected bond lengths and bond angles of compounds **1** and **2** are summarized in Table 2 and Table 3, respectively.

3. Results and discussion

3.1. Structural descriptions of compounds *1* and *2*

Single-crystal X-ray diffraction analysis revealed that compound **1** belongs to the orthorhombic $P2_12_12_1$ space group

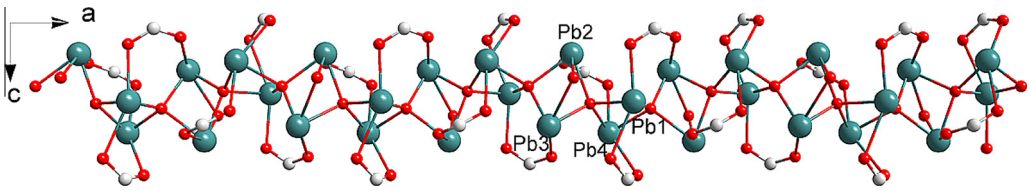

Fig. 2. Ball and stick representation of the infinite 1D rod-shaped SBUs of compound **1**.

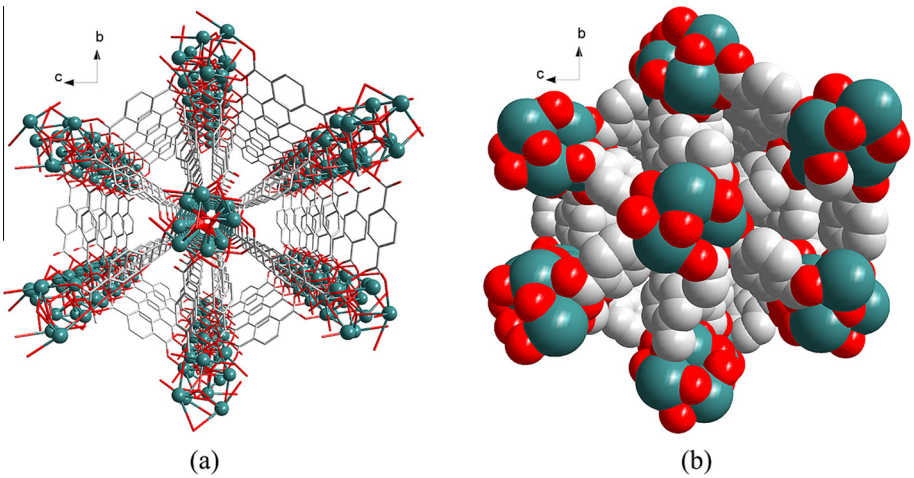

Fig. 3. (a) The 3D open framework and (b) crystal packing structure with 1D channels viewed from the *a* axis of compound **1**. All hydrogen atoms and uncoordinated DMF molecules have been omitted for clarity.

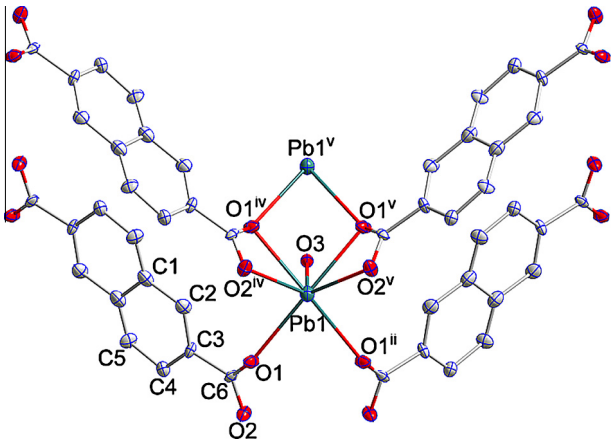

Fig. 4. ORTEP diagram of compound **2** with displacement ellipsoids drawn at 30% probability level. All hydrogen atoms, carbon and nitrogen atoms from coordinated DMF molecules have been omitted for clarity. Symmetry codes: (ii) x, $-y+1/2$, z; (iv) $x+1/2$, y, $-z+1/2$; (v) $x+1/2$, $-y+1/2$, $-z+1/2$.

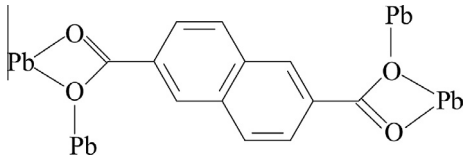

Scheme 2. The coordination mode of ndc ligand in the structure of compound **2**.

(Table 1). The asymmetric unit contains two crystallgraphically independent Pb centers, one bridged oxygen atom, one bdc ligand and one uncoordinated DMF molecule (Fig. 1). Each Pb center is four-coordinate and surrounded by two oxygen atoms from two different bdc ligands and two μ_4-oxo atoms. The coordination geometry of Pb is hemidirected and can be described as a distorted ψ-PbO_4 trigonal bipyramid with the fifth coordination site is occupied by the lone pair of electrons [17]. The Pb–O bond distances are in the range of 2.259–2.757 Å (Table 2). The coordination environment of Pb centers in our case are in agreement with those found in the compound $Pb_7(3\text{-}O_3S\text{–}C_6H_4\text{–}CO_2)(L^1)_3(H_2O)_2{\cdot}2H_2O$ (H_4L^1 = isopropylimino-bis(methylenephosphonic acid) [18]. As shown in Scheme 1, the carboxylate groups of bdc ligands in compound **1** are all deprotonated, and adopt two types of coordination modes (I and II). In mode 1, two carboxylate moieties of the bdc ligand bridges four Pb centers in the bis-bidentate mode, while one carboxylate moiety of bdc in mode II bridges two Pb centers and the other bridges two Pb atoms through one oxygen atom.

As shown in Fig. 2, the ψ-$Pb1O_4$ trigonal bipyramid shares edges (O9, O10) with ψ-$Pb4O_4$ one to form the Pb_2O_6 polyhedron, while ψ-$Pb2O_4$ trigonal bipyramid shares face (O5, O9, O10) with ψ-$Pb3O_4$ one to form the Pb_2O_5 polyhedron. As a result, the Pb_2O_6 and Pb_2O_5 polyhedron are interlinked to each other through μ_4-O atoms (O9, O10) in a corner-sharing fashion to form an infinite rod along the [1 0 0] direction. In fact, these rods can be viewed as infinite secondary building units (SBUs), similar to those observed in Pb-MOFs [19–21]. Each rod-shaped SBU is connected to six neighboring parallel ones through bdc linkers in mode I and mode II, generating the final 3D microporous framework with the I^1O^2 type (Fig. 3) [22]. The solvent accessible void in the structure of compound **1** accounts for approximately 19.8% of the crystal volume calculated [23], and 1D channels along the a axis were occupied by uncoordinated DMF guest molecules.

When the bdc ligand was replaced with ndc, the 3D porous compound **2** was obtained, which crystallized in the orthorhombic space group P_{nma} (Table 1) and the asymmetric unit consists of one Pb center, one ndc ligand and one coordinated DMF molecule (Fig. 4). The holodirected Pb atom is seven-coordinated by six carboxylate oxygen atoms from four ndc ligands and one oxygen atom from one DMF molecule. The Pb–O bond lengths range from 2.507 to 2.727 Å (Table 3). Different from the coordination mode of bdc ligands compound **1**, the ndc ligand in the structure of compound **2** adopts one coordinated mode (Scheme 2), where ndc ligands links four Pb centers with the two chelating/bridging carboxylate groups to form an infinite chains along the [100] direction (Fig. 5). Adjacent chains are further connected together by bdc linkers into a 3D open framework along the a axis with 1D rhombus (9.977 × 20.146 Å of diagonal distances) channels filled with the coordinated DMF molecules (Fig. 6). The solvent accessible void in the structure accounts for approximately 33.7% of the crystal volume. The rhombus channels have been also observed in related

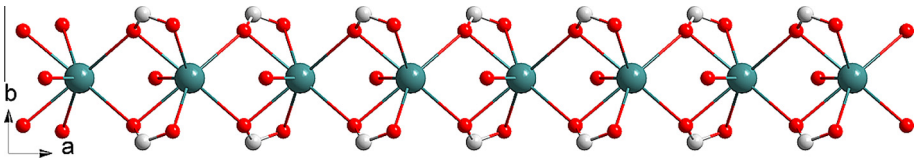

Fig. 5. Ball and stick representation of the infinite 1D rod-shaped SBUs of compound **2**.

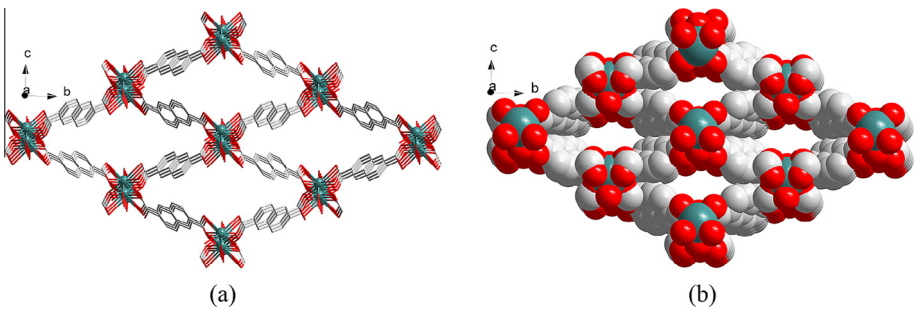

Fig. 6. (a) The 3D open framework and (b) crystal packing structure with rhombus channels viewed from the a axis of compound **2**. Carbon and nitrogen atoms from coordinated DMF molecules, and all hydrogen atoms have been omitted for clarity.

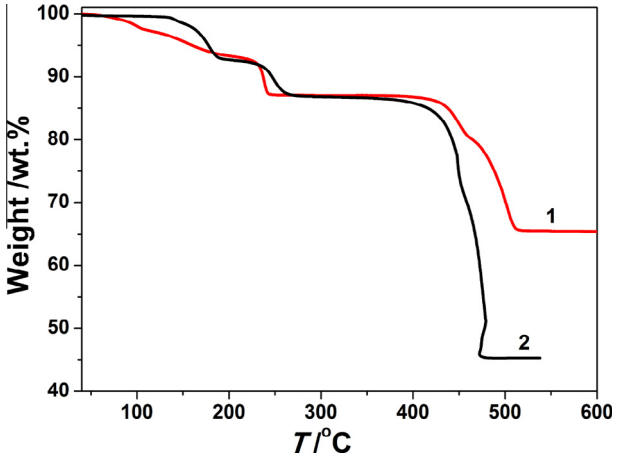

Fig. 7. TG curves of compounds **1** and **2**.

porous MOFs [24]. Obviously, the pore size in compound **2** was much larger than compound **1**.

3.2. TG analysis of compounds *1* and *2*

The initial weight loss (12.55%) between 28 and 242 °C for compound **1** can be attributed to the removal of two crystallized DMF molecules (10.95%) in the structure and the guest-free framework can be maintained up to about 410 °C, above which the framework collapsed (Fig. 7). Similar to compound **1**, the first weight loss (12.77%) between 34 and 265 °C for compound **2** corresponded to the release of one coordinated DMF molecule (14.78%). No weight loss was observed for compound **2** until the decomposition onset temperature of *ca.* 415 °C. Compounds **1** and **2** exhibit residual mass of 65.44% and 45.34%, respectively. However, the compositions of residual phases can not be identified according to the current experimental data.

3.3. Gas sorption properties of compound *1*

As shown in Fig. 8, powder XRD patterns of as-synthesized compounds **1** and **2** are in accordance with those simulated from single-crystal XRD data, indicating the purities of both products. In powder XRD patterns after the adsorption experiments for compound **1**, the main diffraction peaks changed compared with those of the as-synthesized solid. This fact may be due to the deformation of frameworks upon activation. However, the evacuated solids are still stable and retain high periodicity, justified by the sharp diffraction peaks. It should be noted that the framework of compound **2** collapsed significantly upon the removal of solvents, which has been confirmed by the board and weak diffraction peaks after adsorption experiments. So only the gas adsorption isotherms at 77 K of compound **1** were carried out and shown in Fig. 9.

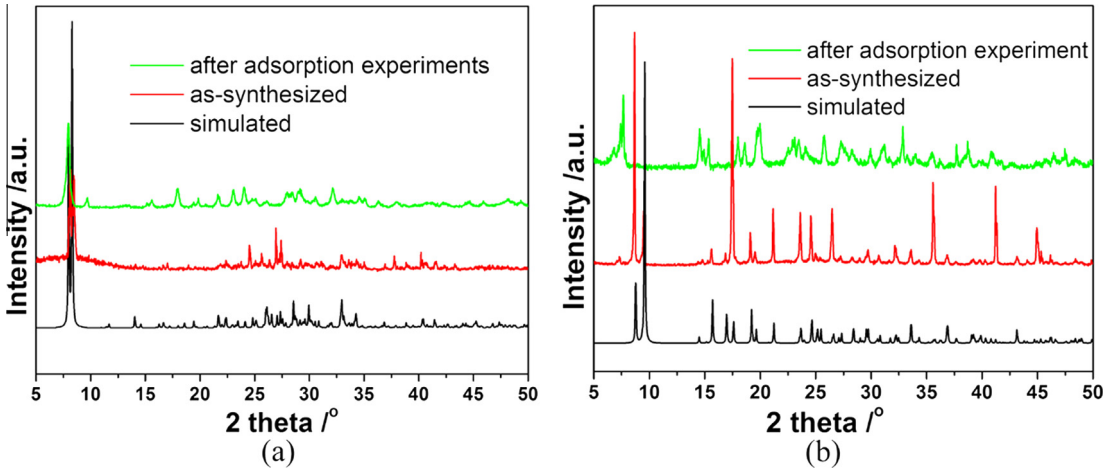

Fig. 8. Powder XRD patterns of simulated, as-synthesized and after adsorption experiments for compounds (a) **1** and (b) **2**.

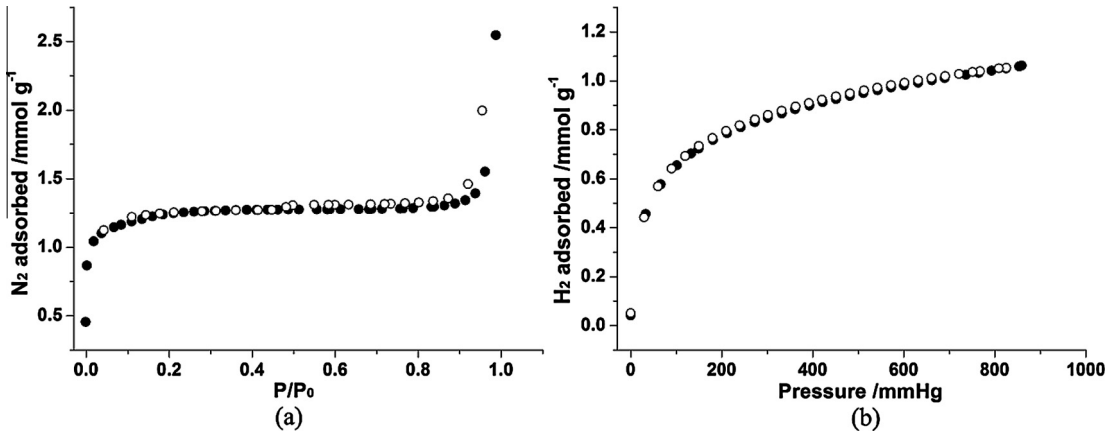

Fig. 9. (a) N_2 and (b) H_2 adsorption/desorption isotherms for compound **1** at 77 K. Solid and open markers indicate adsorption and desorption, respectively.

It should be noted here that nitrogen and hydrogen adsorption characterizations of lead(II) MOFs with polycarboxylate acids have not been reported in literatures to date. Nitrogen sorption/desorption isotherms of compound **1** are classified as type I, typical of microporous materials. A small additional amount at higher pressures is adsorbed, most probably multilayers on the external surface. The surface area from the BET model is 82 m^2 g, lower significantly than those observed for MOF-5 [25]. The hydrogen sorption/desorption isotherms measured at 77 K show fully reversible adsorption and absence of hysteresis. The maximum uptake at 860 mmHg was about 1.1 mmol g. The moderate uptakes for nitrogen and hydrogen gases may be attributed to the existence of micropores in compound **1**, which has also been observed in $[Co(ndc)(azpy)]_2{\cdot}2H_2O{\cdot}DMF$ (azpy = 4,4′-azopyridine) reported by our group [26].

4. Conclusion

We have synthesized two new lead(II) MOFs constructed by aromatic polycarboxylate acids. Both compounds adopt rod-based 3D porous frameworks with 1D channels, and exhibit high thermal stabilities. The existence of micropores in the structure is responsible practically for moderate nitrogen and hydrogen uptakes. Our continuous studies are underway to seek porous lead MOFs with intriguing topologies and interesting sorption properties.

Acknowledgements

This research was supported by National Natural Science Foundation (51072072, 51102119) and Natural Science Foundation of Jiangsu Province (BK2010343, BK2011518).

Appendix A. Supplementary data

CCDC 929256(**1**) and 929257(**2**) contain the supplementary crystallographic data for this paper. Supplementary data associated with this article can be found, in the online version, at http://dx.doi.org/10.1016/j.micromeso.2013.09.035.

References

[1] S.-Q. Ma, H.-C. Zhou, Chem. Commun. 46 (2010) 44–53.
[2] J.-R. Li, R.J. Kuppler, H.-C. Zhou, Chem. Soc. Rev. 38 (2009) 1477–1504.
[3] P. Horcajada, R. Gref, T. Baati, P.K. Allan, G. Maurin, P. Couvreur, G. Férey, R.E. Morris, C. Serre, Chem. Rev. 112 (2012) 1232–1268.
[4] D. Farrusseng, S. Aguado, C. Pinel, Angew. Chem., Int. Ed. 48 (2009) 7502–7513.
[5] M.-L. Hu, A. Morsali, L. Aboutorabi, Coord. Chem. Rev. 255 (2011) 2821–2859.
[6] J.-D. Lin, S.-T. Wu, Z.-H. Li, S.-W. Du, CrystEngComm 12 (2010) 4252–4262.
[7] X.-M. Lin, T.-T. Li, L.-F. Chen, L. Zhang, C.-Y. Su, Dalton Trans. 41 (2012) 10422–10429.
[8] M. O'Keeffe, O.M. Yaghi, Chem. Rev. 112 (2012) 675–702.
[9] F.A.A. Paz, J. Klinowski, S.M.F. Vilela, J.P.C. Tomé, J.A.S. Cavaleiro, J. Rocha, Chem. Soc. Rev. 41 (2012) 1088–1110.
[10] H. Zhou, J.-D. Lin, S.-W. Du, J. Mol. Struct. 930 (2009) 49–54.
[11] W.-T. Liu, Y.-C. Ou, Y.-L. Xie, Z.-J. Lin, M.-L. Tong, Eur. J. Inorg. Chem. (2009) 4213–4218.
[12] M. Liu, Z.-P. Yang, W.-H. Sun, X.-P. Li, J.-S. Ma, G.-Q. Yang, Inorg. Chim. Acta 362 (2009) 2884–2889.
[13] Bruker; SMART, SAINT and XPREP: Area Detector Control and Data Integration and Reduction Software, Bruker Analytical X-ray Instruments Inc., Madison, Wisconsin, USA, 1995.
[14] G.M. Sheldrick, *SADABS: Empirical Absorption and Correction Software*, University of Göttingen, Göttingen, Germany, 1996.
[15] G.M. Sheldrick, SHELXS-97, Program for X-ray Crystal Structure Determination; Göttingen University, Göttingen, Germany, 1997.
[16] G.M. Sheldrick, Acta Crystallogr. A64 (2008) 112–122.
[17] L. Shimoni-Livny, J.P. Glusker, C.W. Bock, Inorg. Chem. 37 (1998) 1853–1867.
[18] S.-M. Ying, J.-G. Mao, Eur. J. Inorg. Chem. (2004) 1270–1276.
[19] S.-C. Chen, Z.-H. Zhang, Q. Chen, H.-B. Gao, Q. Liu, M.-Y. He, M. Du, Inorg. Chem. Commun. 12 (2009) 835–838.
[20] Y.-X. Tan, F.-M. Meng, M.-C. Wu, M.-H. Zeng, J. Mol. Struct. 928 (2009) 176–181.
[21] S.-C. Chen, Z.-H. Zhang, Y.-S. Zhou, W.Y. Zhou, Y.-Z. Li, M.-Y. He, Q. Chen, M. Du, Cryst. Growth Des. 11 (2011) 4190–4197.
[22] A.K. Cheetham, C.N.R. Rao, R.K. Feller, Chem. Commun. (2006) 4780.
[23] A.L. Spek, J. Appl. Crystallogr. 36 (2003) 7–13.
[24] C.-Y. Gao, S.-X. Liu, L.-H. Xie, Y.-H. Ren, R.-G. Cao, J.-F. Cao, X.-Y. Zhao, J. Mol. Struct. 891 (2008) 384–387.
[25] N.L. Rosi, J. Eckert, M. Eddaoudi, D.T. Vodak, J. Kim, M. O'Keeffe, O.M. Yaghi, Science 300 (2003) 1127–1129.
[26] J. Wang, Y. Zhang, X.-Q. Liu, J. Xiao, H. Zhou, A.-H. Yuan, Microporous Mesoporous Mater. 159 (2012) 100–104.